Minimal models for topological Weyl semimetals

Timothy M. McCormick, Itamar Kimchi, and Nandini Trivedi

Phys. Rev. B **95**, 075133 — Published 21 February 2017

DOI: 10.1103/PhysRevB.95.075133

Minimal models for topological Weyl semimetals

Timothy M. McCormick,[1,*] Itamar Kimchi,[2,†] and Nandini Trivedi[1,‡]

[1] *Department of Physics and Center for Emergent Materials, The Ohio State University, Columbus, OH 43210, USA*

[2] *Department of Physics, Massachusetts Institute of Technology, Cambridge, MA 02139, USA*

(Dated: January 27, 2017)

Topological Weyl semimetals (TWS) can be classified as type-I TWS, in which the density of states vanishes at the Weyl nodes, and type-II TWS, in which an electron pocket and a hole pocket meet at a singular point of momentum space, allowing for distinct topological properties. We consider various minimal lattice models for type-II TWS. The simplest time-reversal-breaking band structure, with a pair of Weyl nodes sharing a single electron pocket and a single hole pocket ("hydrogen-model"), exhibits relics of surface Fermi arc states only away from the Fermi energy, with no topological protection. Topologically-protected Fermi arcs can be restored by an additional term ("hydrogen-model") that produces a bulk structure where the electron and hole pockets of each Weyl point are disjoint. In time-reversal-symmetric but inversion-breaking models, we identify non-topological surface "track states" that arise out of the topological Fermi arc states at the transition from type-I to type-II and persist in the type-II TWS. The distinctions among these minimal models can aid in distinguishing between generic and model-dependent behavior in studies of superconductivity, magnetism and quantum oscillations of type-II Weyl semimetals.

PACS numbers: 71.10.Fd,71.18.+y,71.90.+q

I. INTRODUCTION

The band theory of solids was revolutionized by the discovery of topological insulators[1,2]. The abundant list of topologically nontrivial quadratic Hamiltonians has been extended by the recent discovery of topological Weyl semimetals (TWS). These materials have band crossings, at isolated points in momentum space, between two non-degenerate bands. The resulting nodes appear analogous to the Dirac nodes of graphene[3], but here exist in three dimensions rather than two. The three linearly independent momenta couple to all three Pauli matrices in the Hamiltonian, hence perturbations can shift the position of the node in momentum space but cannot open a gap.

There have been many recent theoretical proposals for the emergence of Weyl nodes in the band structure of solid state materials[4–10]. In such a TWS, breaking either inversion or time reversal symmetry results in a pair of Dirac nodes separating into Weyl nodes. These Weyl nodes are monopoles of Berry curvature in the Brillouin zone and the charge associated with such a monopole is known as its chirality. Weyl nodes must come in pairs of opposite chirality[11] such that the net chirality over the Brillouin zone is zero. A consequence of these bulk Weyl nodes is the existence of topological Fermi arcs on the surface of a TWS[7].

Both the bulk Weyl nodes and the surface Fermi arcs have unique signatures in angle resolved photoemission spectroscopy (ARPES) experiments. Searching for these signatures has proven to be extremely fruitful and several groups[12–18] have discovered a TWS phase in the transition metal pnictide family: TaAs, TaP, NbP and NbAs. These materials all belong to the so-called type-I TWS phase where the Weyl points are formed from a direct gap semiconductor closing linearly at a discrete set of Weyl points. A separate class, known as type-II TWS, was recently predicted to arise from an indirect-gap semimetal, with the direct gap closing linearly at the Weyl nodes. These predictions have been made for a variety of compounds[19–22]. Recently, signatures of a type-II TWS have been reported[23–25] in $Mo_xW_{1-x}Te_2$, stoichiometric $MoTe_2$, and LaAlGe, opening the door for further experimental study of the type-II TWS.

Although there have been some studies of lattice models for TWS,[26–28] much of the theoretical work on topological Weyl semimetals has focused on low energy effective models of single Weyl nodes. In a type-I TWS, where the density of states vanishes at the energy of the Weyl nodes, these effective models capture much of the essential physics including electro- and magnetotransport,[29–37] thermoelectric properties,[38–41] magnetic properties,[42] and effects of disorder[43–45]. In a type-I TWS, when the chemical potential is shifted slightly away from the nodal energy, the Fermi pockets enclosing the projections of the Weyl nodes are very small. However, in a type-II TWS extended pockets of holes and electrons exist already at the node energy. Doping away from the node energy then results in the surface projections of the Weyl nodes, for typical crystal surfaces, becoming enclosed within large Fermi pockets. Understanding the interplay of these large Fermi pockets and any topological properties associated with the type-II nodes can require explicit lattice models, rather than just a low-energy theory. Here we present a study of a few such relatively simple lattice models for type-II TWS.

We begin by discussing models for time-reversal-breaking type-II TWS. We distinguish between two types of basic models: the simplest model ("hydrogen-like model") has a single pair of Weyl nodes which share a

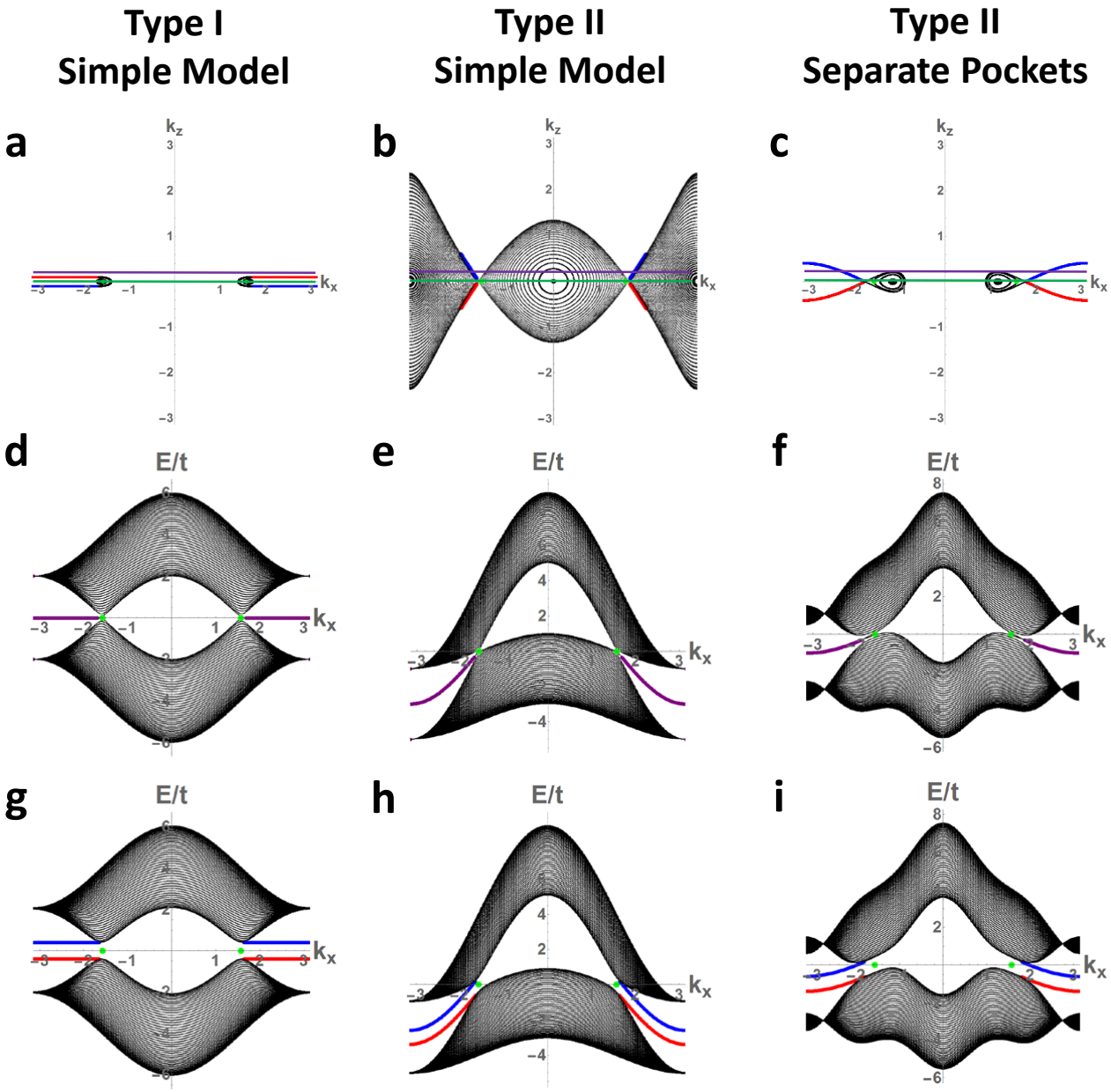

FIG. 1. **Surface and bulk dispersions in the minimal time-reversal-breaking models.** **a-c** Bulk Fermi pockets (black) and surface Fermi arcs (red and blue), shown at $E = -0.2t$, for three models: (**a**) the simplest type-I case (Eq. 8 with $\gamma = 0$), (**b**) the simple two pocket type-II case (Eq. 8 with $\gamma = 3t$), and (**c**) the two node TRB case with isolated pockets surrounding each node ($\gamma = 1.5t$). The thin green and purple lines correspond to the cuts shown in panels (**d-f**) and (**g-i**) respectively. **d-f** Bulk surface dispersions with k_x at $k_z = 0$. Surface states at the top and the bottom surfaces are degenerate and shown in purple. **g-i** Bulk surface dispersions with k_x at $k_z = 0.2$. Surface states at the top and the bottom surfaces are nondegenerate and shown in red and blue respectively.

single electron pocket and a single hole pocket. However, we argue that this simplest model fails to capture some important properties. These are instead captured by the next-simplest model ("helium-like model"), with an additional term that splits both the electron pocket as well as the hole pocket into pairs of separate pockets. Each Weyl node is now formed from the intersection of an isolated pair of electron and hole pockets. The hydrogen-like model has no topologically-protected Fermi arcs, though it exhibits relics of them away from the Fermi energy; in the helium-like model, the topological Fermi arcs are restored. The development of surface states between the models is summarized in Figure. 1. We also study inversion-breaking type-II TWS models,

and find that even simple toy models support an additional set of surface states ("track states") which are not topological but nonetheless play a role, as summarized in Figure. 1, in how the Fermi arc connectivity changes when either the Fermi energy is changed or when the tilt of the Weyl nodes is changed.

The paper is organized as follows. In Sec. II, we outline the general form of the dispersion of a type-II Weyl node and summarize the symmetry properties that a TWS must obey. In Sec. III, we consider the minimal hydrogen and helium models for a time reversal breaking type-II TWS with a single pair of Weyl nodes. In Sec. IV, we consider an inversion breaking model for a type-II Weyl semimetal and study the Fermi arcs as well as the non-topological surface state denoted as "track state." Sec. V contains a discussion of the types of surface states supported by these lattice models, and a discussion of the requirements for Fermi arcs to be topologically protected in a type-II TWS. Sec. VI contains a comparison with experiments. We conclude in Sec. VII with prospects for future investigations.

II. GENERAL CONSIDERATIONS

The defining features of a TWS are the nodal energy crossings in the Brillouin zone, so a minimal lattice model for a TWS must have at least two bands of the form

$$\hat{H} = \sum_{\mathbf{k}} \hat{c}^{\dagger}_{\mathbf{k}\alpha} \left(\hat{\mathcal{H}}(\mathbf{k}) \right)_{\alpha\beta} \hat{c}_{\mathbf{k}\beta} \tag{1}$$

where $\hat{c}^{(\dagger)}_{\mathbf{k}\alpha}$ annihilates (creates) an electron at momentum $\mathbf{k}$ in orbital α and

$$\hat{\mathcal{H}}(\mathbf{k}) = \sum_{i=0,1,2,3} d_i(\mathbf{k})\ \hat{\sigma}_i. \tag{2}$$

Here $\hat{\sigma}_i$ is the i-th Pauli matrix for $i = 1, 2, 3$ whose indices correspond to an orbital degree of freedom and $\hat{\sigma}_0$ is the 2×2 identity matrix. If such a Hamiltonian has at least two points around which the Hamiltonian is described locally by

$$\hat{\mathcal{H}}_{\mathrm{WP}}(\mathbf{k}) = \sum_{i=1,2,3} \gamma_i k_i \hat{\sigma}_0 + \sum_{i,j=1,2,3} k_i A_{ij} \hat{\sigma}_i, \tag{3}$$

it describes a Weyl semimetal with nodes of chirality $\chi = \det(A_{ij})$. It is straightforward to show that the energy spectrum for the Hamiltonian in Eqn. (3) is given by

$$E_{\pm}(\mathbf{k}) = \sum_{i=1,2,3} \gamma_i k_i \pm \sqrt{\sum_{j=1,2,3} \left(\sum_{i=1,2,3} k_i A_{ij} \right)^2} = T(\mathbf{k}) \pm U(\mathbf{k}), \tag{4}$$

where $T(\mathbf{k})$ tilts the Weyl cone. The definition[19,46] of a type-II Weyl node is one where there exists a direction $\mathbf{e_k}$ in the Brillouin zone such that

$$T(\mathbf{e_k}) > U(\mathbf{e_k}). \tag{5}$$

Since in the presence of both inversion and time reversal symmetry the Berry curvature is identically zero throughout the Brillouin zone, the presence of Weyl nodes relies on breaking either inversion (henceforth labeled $\hat{\mathcal{P}}$) or time reversal symmetry (labeled $\hat{\mathcal{T}}$). For spinless fermions, we choose a definite representation for the $\hat{\mathcal{P}}$ and $\hat{\mathcal{T}}$ operators,

$$\hat{\mathcal{P}} \leftrightarrow \hat{\sigma}_1,\ \hat{\mathcal{T}} \leftrightarrow \hat{K}, \tag{6}$$

where $\hat{K}$ is the anti-Hermitian complex conjugation operator. Each of $\hat{\mathcal{P}}$ and $\hat{\mathcal{T}}$ also reverse the sign of the momentum such that $\mathbf{k} \to -\mathbf{k}$. In this paper we investigate lattice models for Weyl semimetals that break either $\hat{\mathcal{T}}$ or $\hat{\mathcal{P}}$, and using the definitions in Eqn. (6) it will be straightforward to show this symmetry breaking explicitly for each model we consider.

III. TIME REVERSAL BREAKING MODEL

We begin by investigating a lattice model given by a Hamiltonian $\hat{\mathcal{H}}(\mathbf{k})$ that hosts Weyl nodes and breaks time reversal symmetry but preserves inversion symmetry such that

$$\hat{\mathcal{P}}^{\dagger} \hat{\mathcal{H}}(-\mathbf{k}) \hat{\mathcal{P}} = \hat{\mathcal{H}}(\mathbf{k}),\ \hat{\mathcal{T}}^{\dagger} \hat{\mathcal{H}}(-\mathbf{k}) \hat{\mathcal{T}} \neq \hat{\mathcal{H}}(\mathbf{k}). \tag{7}$$

The minimal number of Weyl nodes for such a Hamiltonian is two and we find that such a minimal model can be used to investigate a wide range of possible TWS Fermi surface and arc connectivity. We begin by writing down the simplest possible two node time-reversal breaking (TRB) Hamiltonian with a type-II tilt and investigating its band structure. A pair of Weyl nodes are formed from the nodal crossing of exactly one electron band with one hole band. By calculating the band structure for the system in a finite slab geometry, we investigate the surface Fermi arc behavior. We then show that this minimal model can be modified with a term that splits these electron and hole pockets into pairs that exist around each node.

A. The "Hydrogen atom" for a type II time reversal breaking TWS

The following Hamiltonian

$$\hat{\mathcal{H}}_A^{\mathrm{TRB}}(\mathbf{k}) = \gamma\big(\cos(k_x) - \cos(k_0)\big)\hat{\sigma}_0 - \big(m(2 - \cos(k_y) - \cos(k_z)) + 2t_x(\cos(k_x) - \cos(k_0))\big)\hat{\sigma}_1 - 2t\,\sin(k_y)\hat{\sigma}_2 - 2t\,\sin(k_z)\hat{\sigma}_3 \quad (8)$$

satisfies the symmetry conditions in Eqn. (7) and possesses two Weyl nodes at $\mathbf{k} = (\pm k_0, 0, 0)$. When $\gamma = 0$, this Hamiltonian is known[47] to host nodes of type-I. However, the addition of the term $\gamma\big(\cos(k_x) - \cos(k_0)\big)\hat{\sigma}_0$ bends both bands and when $\gamma > 2t_x$ it is simple to see these nodes become type-II as defined by Eqn. (5). We see this evolution from type-I to type-II very clearly in Fig. 2. When $\gamma = 0$, the hole band (blue) touches the electron band (red) at the two Weyl points where the density of states vanishes, as seen in Fig. 2a,d,g. When the system is in the type-II regime, the Weyl cones are tilted and this leads to a nonzero density of electron and hole states at the node energy, as seen clearly in Fig. 2c,f,i. When $\gamma = 2t_x$ exactly, the system is at a critical point between a type-I and a type-II Weyl semimetal. This is clearly seen in Fig. 2b,e,h, where a single line of bulk states connect the Weyl points at $E = 0$. The states seen in Fig. 2h open up into the electron and hole pockets seen at $E = 0$ for the type II case in Fig. 2i.

In a type-II TWS, it is important to consider the net chirality enclosed by the bulk Fermi pockets when determining the Fermi arc connectivity. If one encloses a bulk pocket by a Gaussian surface in a region where the bulk band structure is gapped, the number of Fermi arcs impinging on the Gaussian surface are quantized and equal to the net chirality of Weyl nodes enclosed. When the model in Eqn. (8) is in the type-II regime and the chemical potential is shifted away from $E = 0$, the projections of both Weyl nodes are either enclosed in the electron pocket ($E > 0$) or the projections are both enclosed in the hole pocket ($E < 0$). Since the projections of both nodes lie within the same Fermi pocket, we expect that Fermi arcs in this system are not topologically protected in general. Surface states may exist, but their lack of topological protection stems from the fact that there are no isolated Fermi pockets that enclose Weyl nodes with nonzero net chirality. As a result, the surface states can hybridize with bulk states and are therefore trivial.

In order to investigate the structure of the Fermi arcs, we introduce an edge by considering a slab with a finite thickness in one direction. We partially Fourier transform the Hamiltonian in Eqn. (8) into real space for a L layer system in the y-direction, while keeping the system infinite in the x- and z-directions. In Fig. 3, we show the results of such a slab calculation for the model given by Eqn. (8) in the type I regime ($\gamma = 0$) with the same bulk parameters as in Fig. 2a,d,g and in the type II regime ($\gamma = 3t_x$) with the same bulk parameters as in Fig. 2c,f,i for $L = 50$ layers. We calculate the expectation of the finite position $\langle y\rangle$ and label the states as "top" ("bottom") if they are exponentially localized at $\langle y\rangle = 1$ ($\langle y\rangle = L$). We color these top and bottom states red and blue respectively.

As we expect, for the type-I case when $\gamma = 0$, a Fermi arc on each surface connects the Weyl nodes, as seen in Fig. 3a-c. This is seen clearly in Fig. 3b where two Fermi arcs connect the two nodes from $(k_x, k_z) = (-\pi/2, 0)$ to $(k_x, k_z) = (\pi/2, 0)$. At $E = 0$, both the top and bottom arcs are degenerate at $k_z = 0$, shown as a purple line. When we lower the Fermi energy below the node energy, each node is enclosed in a small isolated Fermi pocket. Since each pocket encloses a net chirality $\chi = \pm 1$, the pockets are connected by an arc on each surface, as seen in Fig. 3a. The same is seen at higher energies $E > 0$ in Fig. 3c.

We calculate the band structure in the slab geometry for a type-II TWS ($\gamma = 3t_x$) and find that there are marked differences in the surface state behavior (see Fig. 3d-f). Since both nodes are formed from a single electron and a single hole pocket, we cannot construct a simply connected 2D Gaussian surface in the Brillouin zone that encloses a single node. When the energy is lower than the Weyl energy in Fig. 3d, we see that the projections of both nodes are enclosed by the same hole pocket. Although there are two sets of surface states connecting the hole and electron pockets, they are trivial in a topological sense. When one considers a Gaussian surface that encloses the central hole pocket, it is pierced by four arcs, two on each real-space surface. The Fermi velocity of each arc is opposite on a given real-space surface and so the net chirality of the arcs is zero. We see that as we raise the chemical potential to the node energy and above, these arcs disappear completely. This is completely different from the type-I case where the arcs exist at all energies since the nodes were always isolated in separate Fermi pockets.

B. The "Helium atom" for a type II time reversal breaking TWS

In order to study the physics of type-II Weyl nodes surronded by isolated Fermi pockets which they do not share, we seek to introduce a term to the Hamiltonian separates the single pair of pockets possessed by the "Hydrogen-atom" model. In particular, this new term must gap out the bulk band structure in the $k_x = 0$ plane and the $k_x = \pi$ plane. Due to the pairs of electron and hole pockets supported by this model, we call it the "Helium model" for a type-II time-reversal-breaking TWS in analogy with the "Hydrogen model" above. We consider the following Hamiltonian

$$\hat{\mathcal{H}}_B^{\mathrm{TRB}}(\mathbf{k}) = \hat{\mathcal{H}}_A^{\mathrm{TRB}}(\mathbf{k}) - \gamma_x(\cos(3k_x) - \cos(3k_0))\hat{\sigma}_1, \quad (9)$$

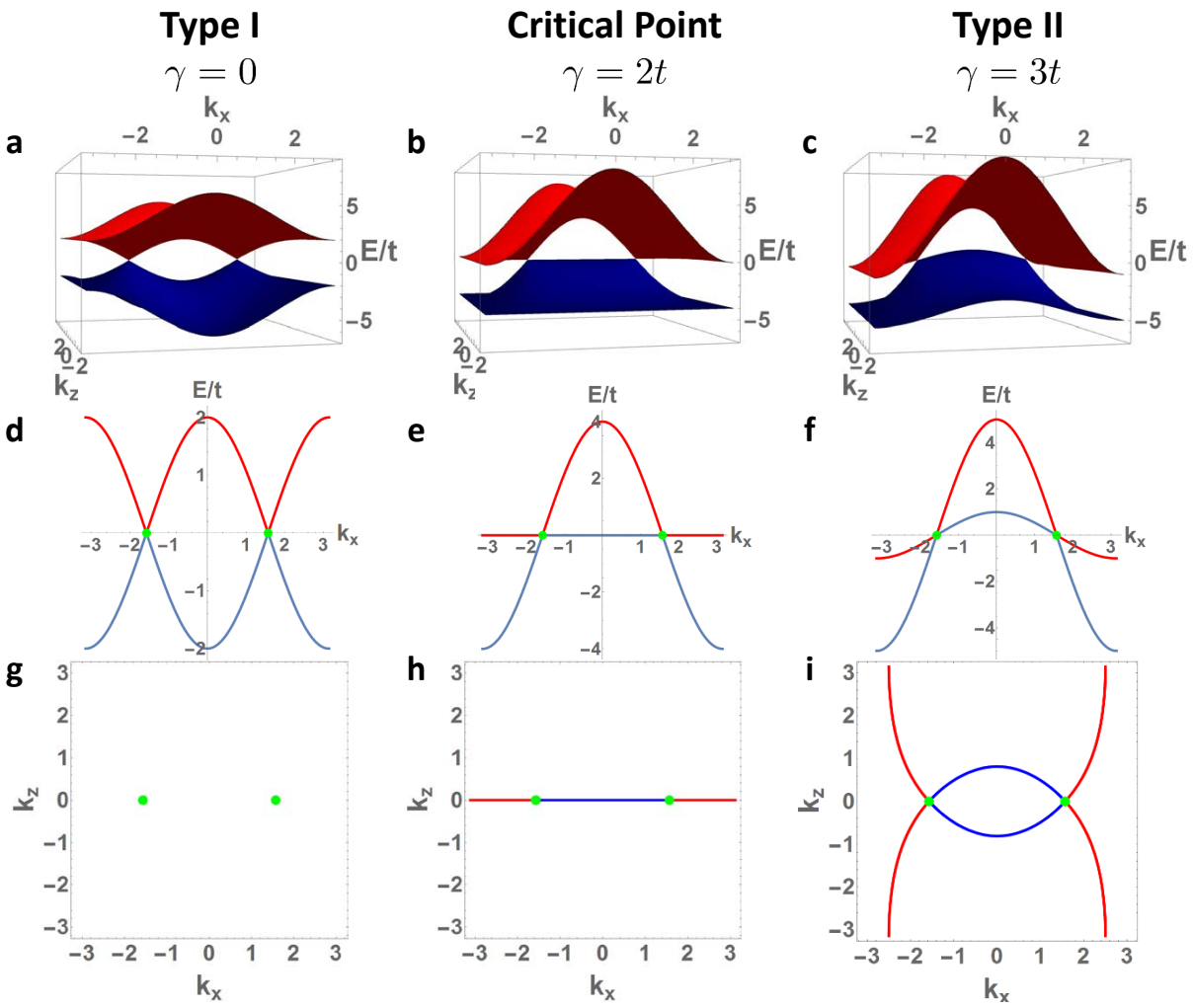

FIG. 2. **Bulk band structure for the "Hydrogen atom" of type-I and type-II Weyl semimetal.** **a-c** The bulk band structure for the Hamiltonian in Eqn. (8). Electron pockets shown in red and hole pockets shown in blue merge at the Weyl nodes shown in green. Here we have chosen parameters $k_y = 0$ with parameters $k_0 = \pi/2$, $t_x = t$, $m = 2t$ for (**a**) type-I Weyl semimetal with $\gamma = 0$, (**b**) the critical point between type-I and type-II Weyl semimetal with $\gamma = 2t$ and (**c**) type-II Weyl semimetal with $\gamma = 3t$. The cones comprising the Weyl nodes develop a characteristic tilt of the type-II TWS as γ is increased. **d-f** Cuts through the Weyl nodes at $k_y = k_z = 0$ for the same parameters as (**a-c**). **g-i** Constant energy cuts through the nodal energy ($E = 0$) for the same parameters as (**a-c**). We see that for a type-I TWS, there are no states at the Fermi energy. At the critical point between a type-I and type-II TWS, we see lines of bulk states appearing between the nodes. These lines open into bulk hole and electron pockets (in the repeated zone scheme) when the system becomes a type-II TWS.

where we have added to Eqn. (8) the term proportional to γ_x. In general, this model supports up to six Weyl nodes. However, so long as $|2t_x| > |3\gamma_x|$, there are only two Weyl nodes in the Brillouin zone. These nodes are located at $E = 0$ and $\mathbf{k} = (\pm k_0, 0, 0)$ and they are type-II if $\gamma > 3\gamma_x - 2t_x$. The addition of the term $\gamma_x(\cos(3k_x) - \cos(3k_0))$ gaps out the bulk spectrum along the lines $(k_y, k_z) = (0, 0)$ and $(k_y, k_z) = (0, \pi)$ at the nodal energy. This leads to a pair of isolated hole pockets touching a pair of isolated electron pockets at the Weyl nodes when the system is type-II. In Fig. 4, we find that as γ grows relative to $3\gamma_x - 2t_x$, the Fermi pockets grow in size. This is because as the tilt of the nodes gets larger, more electron and hole states exist at the Fermi energy. As we shift the chemical potential away from the node energy, the projections of the nodes are now isolated with each node in a single electron (hole) pocket when the chemical potential is raised (lowered).

We again consider the slab geometry described in the section above in order to investigate the interplay of the bulk pockets and the Fermi arcs for the model given by Eqn. (9). Unlike the simpler model described by Eqn. (8), we see in Fig. 5 that Eqn. (9) supports isolated Fermi pockets enclosing the Weyl nodes in the type-II regime when $\gamma = t$ (Fig. 5a-c) and $\gamma = 1.5t$ (Fig. 5d-f). Unlike the Fermi surfaces and arcs generated by Eqn. (8), in Fig. 5 we see that each node is isolated in its own hole (Fig. 5a,d) or electron (Fig. 5c,f) pocket when the

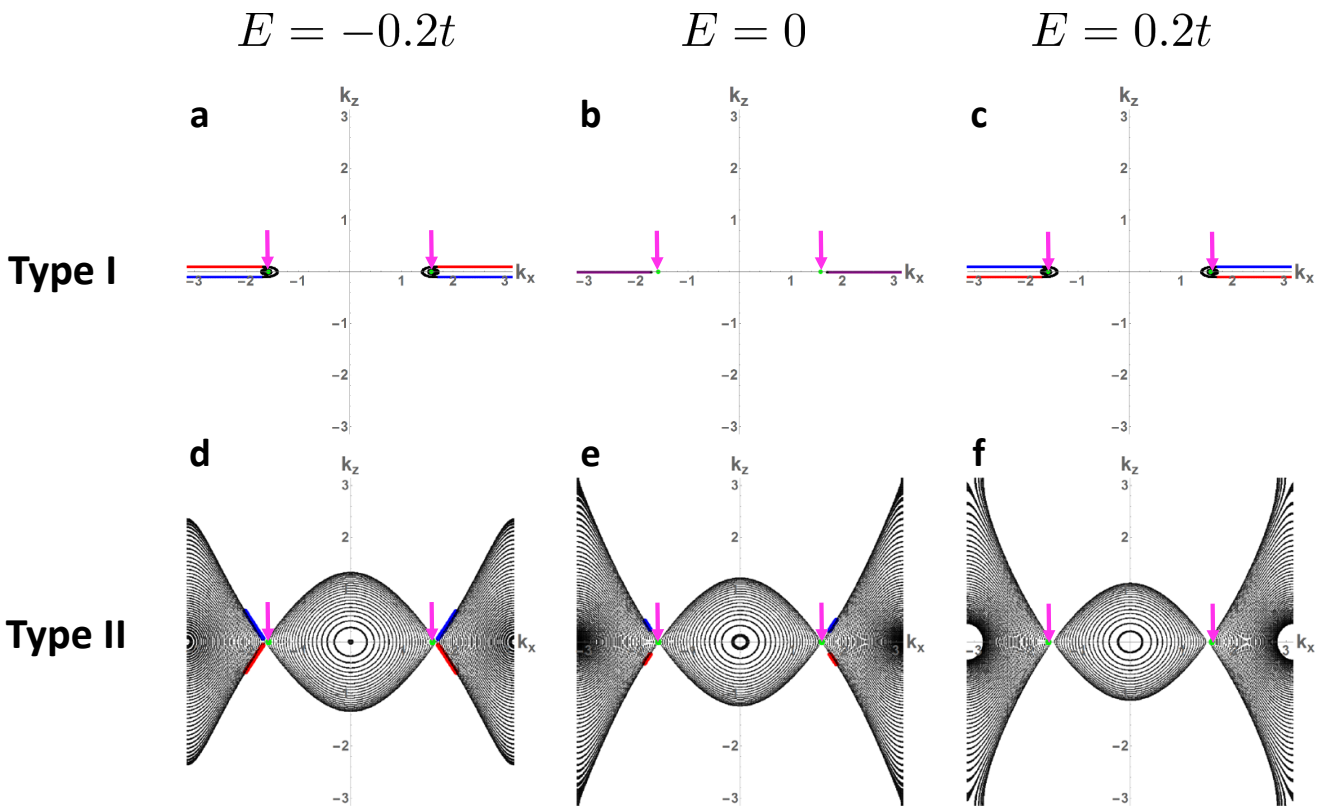

FIG. 3. **Fermi surface and arc configuration for the "Hydrogen atom" of type-I and type-II TWS. a-c** Bulk Fermi surfaces and surface Fermi arcs for a type I TWS with the same bulk parameters as in Fig. 2a,d,g calculated in a slab geometry with $L = 50$ layers in the y-direction. The slab calculations are done at the following constant energy: **(a)** $E = -0.2t$, **(b)** $E = 0$, **(c)** $E = 0.2t$. We color the states which are exponentially localized to the $y = 1$ ($y = L$) surface red (blue) and note that such surface states form topological arcs connecting the two Weyl nodes (shown as green dots and marked with pink arrows). We note that at $E = 0$ the two Fermi arcs are degenerate along $k_z = 0$ and we color them purple to signify this. **d-f** Bulk Fermi surfaces and surface Fermi arcs for a type-II TWS with the same bulk parameters as in Fig. 2c,f,i calculated in a slab geometry with $L = 50$ layers in the y-direction. The slab calculations are done at the same constant energies as above: **(d)** $E = -0.2t$, **(e)** $E = 0$, **(f)** $E = 0.2t$.

chemical potential is away from $E = 0$. We emphasize that this is due to the extra $\hat{\sigma}_1$ term in the Hamiltonian in Eqn. (9). These isolated pockets in Fig. 5 are connected by arcs confined to the surface in the y-direction. However, in this type-II TWS the Fermi pockets enclosing a Weyl node can be quite extended and, unlike a type-I TWS, the arcs can terminate on a pocket quite far away from the projection of the nodes. We see that as the tilt grows in Fig. 5d-f, so do the pockets enclosing the nodes. We note that a trivial electron pocket appears around the $(k_x, k_z) = (\pi, \pi)$ point. This pocket encloses no Weyl nodes and therefore it is not connected via Fermi arcs to any other pockets.

Although the local linearized Hamiltonian describing the spectrum close to a node in Eqn. (9) is identical to the effective Hamiltonian of nodes of the model described by Eqn. (8), the full lattice models describe topologically distinct configurations of bulk Fermi surfaces and surface Fermi arcs. When there is only one electron pocket and one hole pocket with the projections of the Weyl nodes enclosed by the same pocket, the topological protection of the Fermi arcs is lost. However, we see that once each node is enclosed in its own isolated pocket, the topological protection of the Fermi arcs is restored.

Finally, we consider the energy dispersion of the Fermi arcs near a node. Again using the slab geometry as above, we calculate the energy spectrum, this time at a constant k_z, as shown in Fig. 1. We see that for the simplest type-I case (Eqn. (8) with $\gamma = 0$), the surface arcs do not disperse in k_x for a fixed k_z. This changes in the type-II case for both the simple Hamiltonian in Eqns. (8) and (9). At fixed k_z, the arcs connecting the node inherit the tilt proportional to γ and now bend. This characteristic bend of the Fermi arc dispersion has been observed in ARPES studies of type-II Weyl semimetal[24].

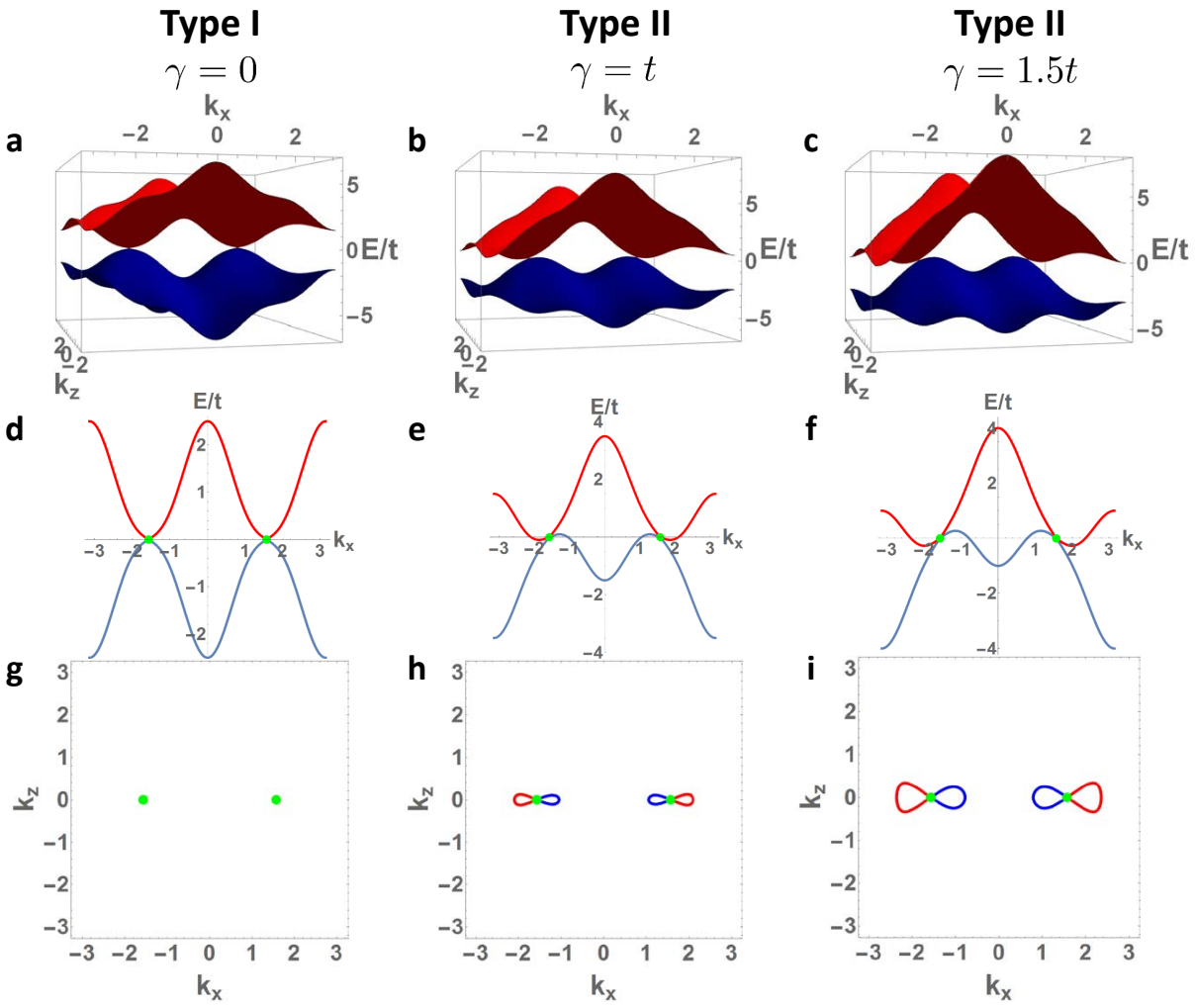

FIG. 4. **Bulk band structure for type-I and type-II TRB model with separate pockets (the "Helium atom").** **a-c** The bulk band structure for the Hamiltonian in Eqn. (9). Electron pockets shown in red and hole pockets shown in blue merge at the Weyl nodes shown in green. Here we have chosen parameters $k_y = 0$ with the parameters $k_0 = \pi/2$, $t_x = t$, $m = 2t$ and $\gamma_x = t/2$ for (**a**) type-I TWS with $\gamma = 0$, (**b**) type-II TWS with $\gamma = t$ and (**c**) type-II TWS with $\gamma = 1.5t$. The cones comprising the Weyl nodes again develop a characteristic tilt of the type-II TWS as γ is increased. **d-f** Cuts through the Weyl nodes at $k_y = k_z = 0$ for the same parameters as (**a-c**). **g-i** Constant energy cuts through the nodal energy ($E = 0$) for the same parameters as (**a-c**). Note that for a type-I TWS, there are no states at the Fermi energy while in the type-II regime, there are two sets of electron and hole pockets on either side of the Weyl nodes. We see that unlike the Hydrogen-atom model, the Helium-atom model has disjoint pairs of electron and hole pockets and a pair of each meet at the two Weyl nodes.

IV. INVERSION BREAKING MODEL

We now turn to a lattice model for a topological Weyl semimetal that breaks inversion symmetry but is invariant under time-reversal. Analogous with Eqn. (7), we seek a Hamiltonian $\hat{\mathcal{H}}(\mathbf{k})$ that satisfies the following symmetry conditions

$$\hat{\mathcal{P}}^\dagger \hat{\mathcal{H}}(-\mathbf{k})\hat{\mathcal{P}} \neq \hat{\mathcal{H}}(\mathbf{k}),\ \hat{\mathcal{T}}^\dagger \hat{\mathcal{H}}(-\mathbf{k})\hat{\mathcal{T}} = \hat{\mathcal{H}}(\mathbf{k}), \qquad (10)$$

where $\hat{\mathcal{P}}$ and $\hat{\mathcal{T}}$ are again given by Eqn. (6). Unlike a time-reversal-breaking Weyl semimetal, the minimum number of Weyl nodes for a spinless inversion-breaking (IB) TWS is four. More importantly, the lattice model for an IB TWS exhibits what we term "track states" that are loops of states that live on the surface of the TWS and are degenerate with the states forming the topological Fermi arcs. However, unlike topological Fermi arcs, these track states form closed contours rather than open ones; they are not topological, but do evolve from the topological arc states upon the transition from type-I to type-II.

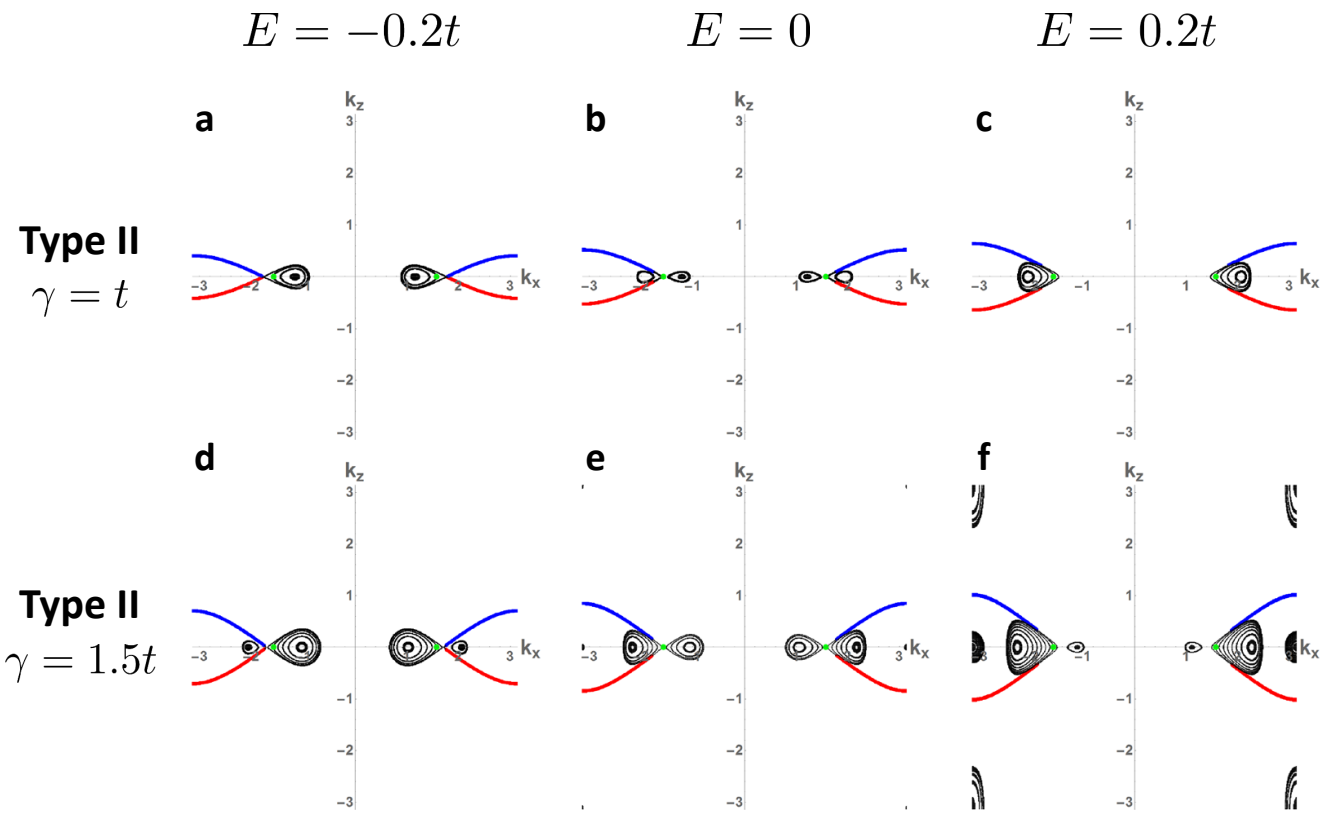

FIG. 5. **Fermi surface and Fermi arc configuration for type I and type-II time-reversal-breaking model with separate pockets (the "Helium atom").** **a-c** Bulk Fermi surfaces and surface Fermi arcs for a type-II Weyl semimetal given by Eqn. (9) with the same bulk parameters as in Fig. 4b,e,h calculated in a slab geometry with $L = 50$ layers in the y-direction. The slab calculations are done at the constant energies: **(a)** $E = -0.2t$, **(b)** $E = 0$, **(c)** $E = 0.2t$. As in Fig. 3, we color the states that are exponentially localized to the $y = 1$ ($y = L$) surface red (blue) and note that such surface states form topological arcs connecting the two Weyl nodes (shown as green dots). We note unlike in Fig. 3, each node is isolated in its own hole (**a**) or electron (**c**) pocket when the chemical potential is away from $E = 0$. These pockets are connected by arcs confined to the surface in the y-direction. However, in this type-II TWS the Fermi pockets enclosing a Weyl node can be quite extended, unlike a type-I TWS, the arcs can terminate on a pocket quite far away from the projection of the nodes. **d-f** Bulk Fermi surfaces and surface Fermi arcs for a type-II TWS with the same bulk parameters as in Fig. 4c,f,i calculated in a slab geometry with $L = 50$ layers in the y-direction. The slab calculations are done at the same constant energies as above: **(d)** $E = -0.2t$, **(e)** $E = 0$, **(f)** $E = 0.2t$. We see that as the tilt grows, so do the pockets enclosing the nodes. We note that a trivial electron pocket appears around the $(k_x, k_z) = (\pi, \pi)$ point. This pocket encloses no Weyl nodes and so is not connected via Fermi arcs to any other pockets.

It is easy to show that the Hamiltonian

$$\hat{\mathcal{H}}^{\mathrm{IB}}(\mathbf{k}) = \gamma(\cos(2k_x) - \cos(k_0))(\cos(k_z) - \cos(k_0))\hat{\sigma}_0 - (m(1 - \cos^2(k_z) - \cos(k_y)) + 2t_x(\cos(k_x) - \cos(k_0)))\hat{\sigma}_1 - 2t\,\sin(k_y)\hat{\sigma}_2 - 2t\,\cos(k_z)\hat{\sigma}_3 \quad (11)$$

satisfies the conditions in Eqn. (10). When $\gamma = 0$, Eqn. (11) describes a TWS with four nodes located at $\mathbf{k}_{\mathrm{W}} = (\pm k_0, 0, \pm\pi/2)$ that breaks inversion but preserves time-reversal symmetry. The term $\gamma(\cos(2k_x) - \cos(k_0))(\cos(k_z) - \cos(k_0))\hat{\sigma}_0$ causes a different shift in both band than those considered in the time reversal breaking cases and results in both bands bending in both the k_x- and k_z-directions. This can produce isolated Fermi pockets around the Weyl points without having to add an additional $\hat{\sigma}_1$ term like in the time-reversal-breaking case in Eqn. (9). The inversion-breaking model above also easily generates trivial Fermi pockets that exist in isolation from those that meet at the Weyl nodes.

We show the bulk band structure for Eqn. (11) in Fig. 6. We see that indeed when $\gamma = 0$ (Fig. 6a,d,g), the electron band meets the hole band at four isolated type-I Weyl points and the density of states vanishes at the nodal energy. As γ increases, the Weyl nodes begin to tilt in the k_z-direction. When γ is tuned to the critical point between the type-I and type-II phases (Fig. 6b,e,h), the electron and hole pockets still meet at the four Weyl nodes with a vanishing density of states, but we see in

Fig. 6e that the Weyl nodes are now tilting in the k_z-direction. As γ is further increased into the type-II limit (Fig. 6c,f,i), we now see that the nodes are tilted as seen in Fig. 6f and the electron (hole) pockets are shifted below (above) the node energy. In particular, we see in Fig. 6i that there are four electron and four hole pockets that exist at $E = 0$ and meet at the Weyl nodes. There is also a trivial hole pocket centered at $\mathbf{k} = (0, 0, 0)$ and a trivial electron pocket centered at $\mathbf{k} = (\pi, 0, 0)$.

In order to study the Fermi arcs, we again construct a slab geometry by transforming the terms dependent on k_y in Eqn. (11) into real space and considering a system with L layers in the y-direction and infinite in the x- and z-directions. In the type-I limit with $\gamma = 0$ shown in Fig. 7a and b, we find that away from $E = 0$, the projections of the nodes are enclosed by isolated small Fermi pockets. These pockets are connected to one another by topological Fermi arcs in the k_x-direction. At $E = 0$, the top and bottom arcs are degenerate along the lines $k_z = \pm\pi/2$. In a sense, this type-I ($\gamma = 0$) limit in the inversion-breaking model is effectively composed of two copies of a time-reversal-breaking Weyl semimetal separated by π reciprocal lattice vectors along the k_z direction.

When γ is increased to the type-II limit, the Fermi arc and bulk Fermi surface configuration in the inversion-breaking case is very different from the time-reversal-breaking model as we see in Fig. 7c and d. The projections of the Weyl nodes are now enclosed by extended hole pockets for $E < 0$ (Fig. 7c) and electron pockets for $E > 0$ (Fig. 7d). These Fermi pockets are connected by topological Fermi arcs, shown by thick red and blue lines, to pockets containing Weyl nodes of opposite chirality. Unlike in the type-I limit, here the Fermi arcs connect pockets along the k_z-direction rather than the k_x-direction. One might expect that the transition point where the Fermi arcs connect nodes in one direction rather than another is concurrent with the transition point between a type-I and type-II Weyl semimetal and indeed our numerical calculations show that is the case (see Fig. 8). Hence we see that for the same model with all other parameters held constant, merely tilting the nodes can lead to a dramatic recombination of the Fermi arcs and a qualitatively different pocket connectivity.

In Fig. 7c and d, we see that there are many states that are exponentially localized on the surface, however many of them form closed loops. We term these closed loops "track states"; they are degenerate in energy with the Fermi arcs but do not share their topology. Unlike Fermi arcs, track states form closed rather than open contours of surface states. By investigating the evolution of the Fermi arc and Fermi surface configuration as a function of γ (Fig. 8), we see that when the Fermi arc connectivity changes from the the k_x-direction to the k_z-direction, they leave behind track states around the $(k_x, k_z) = (\pi, \pi)$ point.

V. SURFACE STATES: TOPOLOGICAL AND TRACK

We briefly recapitulate the argument[7] for the existence of topologically protected Fermi arcs in a Weyl semimetals. It can be shown that a Weyl node is a monopole source of Berry curvature with charge equal to its chirality χ. We enclose an isolated Weyl node by a closed 2D subspace of the Brillouin zone. It is well known that the integral of Berry curvature over a 2D manifold is a quantized integer known as the Chern number[48] when the bulk band structure is gapped over the region of integration. In the case of a surface enclosing a Weyl node, the Chern number calculated in this way is equal to the chirality χ of the node enclosed. By definition, such a surface enclosing a Weyl node defines a 2D Chern insulator and therefore possesses $|\chi|$ chiral edge modes on its boundary. As we consider various families of such closed surface in the Brillouin zone, these chiral edge modes trace out the open contours of surface states known as Fermi arcs that must terminate on Weyl nodes. In this way, there is a correspondence between the Berry curvature of the Weyl nodes, a topological property of the bulk, and the surface Fermi arcs (see sketch in Fig. 9a) that are also topological in nature.

A. Topological Protection of Fermi Arcs in Type-II Weyl Semimetals

The chirality and Berry curvature of a Weyl node are unaffected by its type[19]. In the case of the lattice models we consider in the sections above, this can be shown explicitly by noting that the ith component of the Berry curvature of each band (E_+ and E_-) is given by

$$\Omega_{\mathbf{k},\pm,i} = \pm\epsilon_{ijl}\frac{\mathbf{d_k}\cdot\left(\frac{\partial\mathbf{d_k}}{\partial k_j}\times\frac{\partial\mathbf{d_k}}{\partial k_l}\right)}{4|\mathbf{d_k}|^3}, \qquad (12)$$

where ϵ_{ijl} is the rank 3 Levi-Civita tensor and $\mathbf{d_k} \equiv (d_1(\mathbf{k}), d_2(\mathbf{k}), d_3(\mathbf{k}))$ as defined in Eqn. (2). Since the type of the Weyl node is determined by $d_0(\mathbf{k})$ which does not enter Eqn. (12), the Berry curvature around a node is indeed manifestly invariant with respect to its type.

The presence of topologically protected Fermi arcs relies on the quantized edge modes of 2D surfaces enclosing Weyl nodes. We again emphasize that it is necessary for such 2D surface to exist in a region which is fully gapped in the bulk. If one constructs such a surface which intersects a bulk pocket, then it no longer describes a Chern insulator and the quantization of the edge modes is destroyed. It is clear that the extended pockets around type-II Weyl nodes play an important role in the nature of the connectivity of the Fermi arcs and the pockets, since by definition one necessarily cannot take a gapped 2D surface to lie within these pockets. Therefore, the presence of Fermi arcs in a type-II Weyl semimetal is

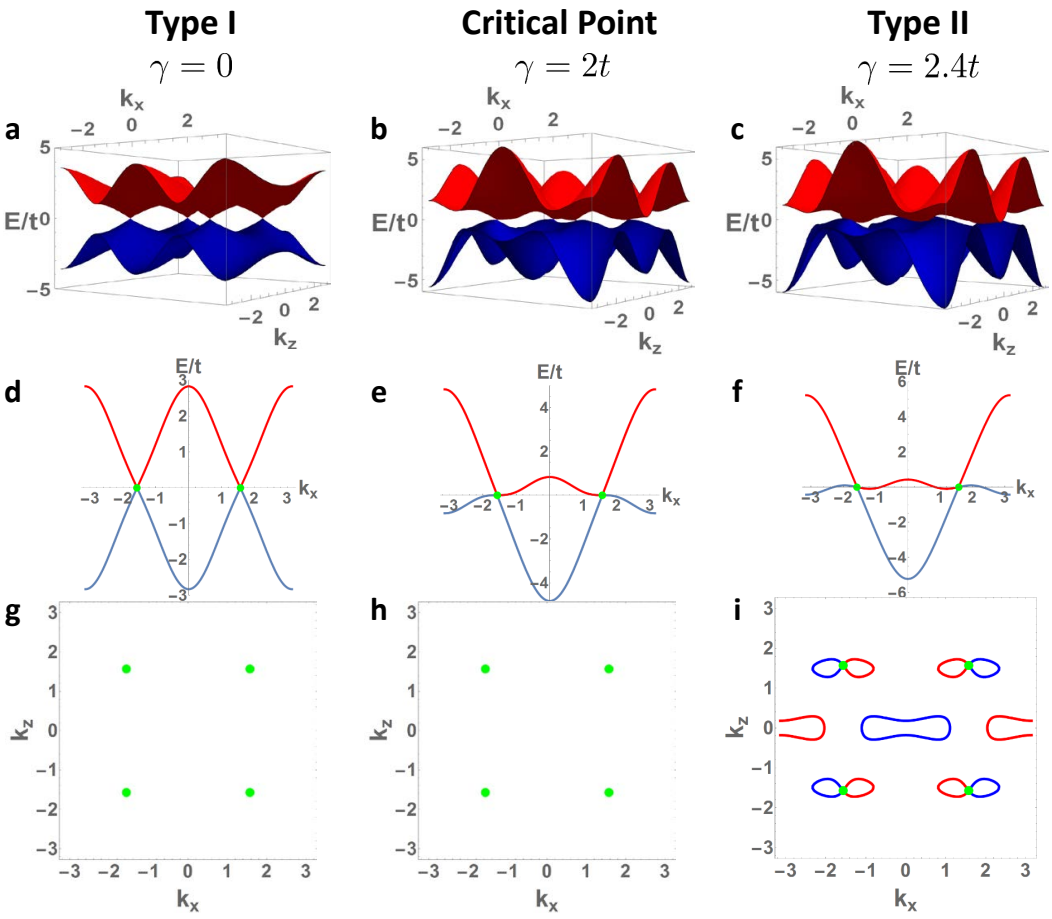

FIG. 6. **Bulk band structure for type-I and type-II inversion breaking TWS. a-c** The bulk band structure for the Hamiltonian in Eqn. (11). Electron pockets shown in red and hole pockets shown in blue merge at the Weyl nodes shown in green. Here we have chosen parameters $k_y = 0$ with the parameters $k_0 = \pi/2$, $t_x = t/2$, $m = 2t$ for (**a**) type I TWS with $\gamma = 0$, (**b**) the critical point between a type-I and a type-II TWS with $\gamma = 2t$ and (**c**) type-II TWS with $\gamma = 2.4t$. The cones comprising the Weyl nodes develop a characteristic tilt of the type-II Weyl node as γ is increased. **d-f** Cuts through the Weyl nodes at $k_y = 0$ and $k_z = -\pi/2$ for the same parameters as (**a-c**). These cuts are shown as the green lines in (**g-i**). **g-i** Constant energy cuts through the nodal energy ($E = 0$) for the same parameters as (**a-c**). We see that for a type-I Weyl semimetal, there are no states at the Fermi energy. At the critical point between a type-I and type-II TWS, the density of states still vanishes. In the type-II regime, electron and hole pockets form near the Weyl nodes. These pockets enclose the projections of the Weyl nodes when the chemical potential is shifted away from $E = 0$. Trivial pockets also appear at $\mathbf{k} = (0, 0, 0)$ and $\mathbf{k} = (0, 0, \pi)$.

only guaranteed by ensuring that the Gaussian surfaces one constructs in the Brillouin zone enclose Fermi pockets rather than bare nodes.

We provide a simple counting argument that limits the possible connectivity of Fermi arcs in a Weyl semimetal of either type:

1. If a Weyl node is type-I with chirality χ, then $|\chi|$ pairs of Fermi arcs will terminate on the Weyl point when the Fermi energy lies at the nodal energy. This well-known result is illustrated for the lattice models in Fig. 3b.

2. If an isolated Fermi pocket fully encloses n Weyl node of either type such that a closed 2D subspace where the bulk band structure is gapped can completely surround the pocket, then the Fermi arcs on a given surface will have net chirality χ_{tot} and terminate on the pocket. Here χ_{tot} is the total chirality of all Weyl nodes enclosed by the Fermi pocket such that $\chi_{tot} = \sum_{i=1}^{n} \chi_i$. For type-I nodes, this is illustrated by Fig. 3a,c and Fig. 7a,b. The lattice models illustrate Fermi pockets enclosing the projections of isolated type-II Weyl nodes in Fig. 5a,c,d,f and Fig. 7c,d. We see in Fig. 3d,f that when the net chirality enclosed is zero, Fermi arcs are not present.

3. When the chemical potential lies at the energy of a type-II Weyl node at least two Fermi pockets are connected at the Weyl node. In this case, it is necessary to consider the set of all connected Fermi pockets when determining the possible Fermi arc configuration. When multiple Weyl nodes connect

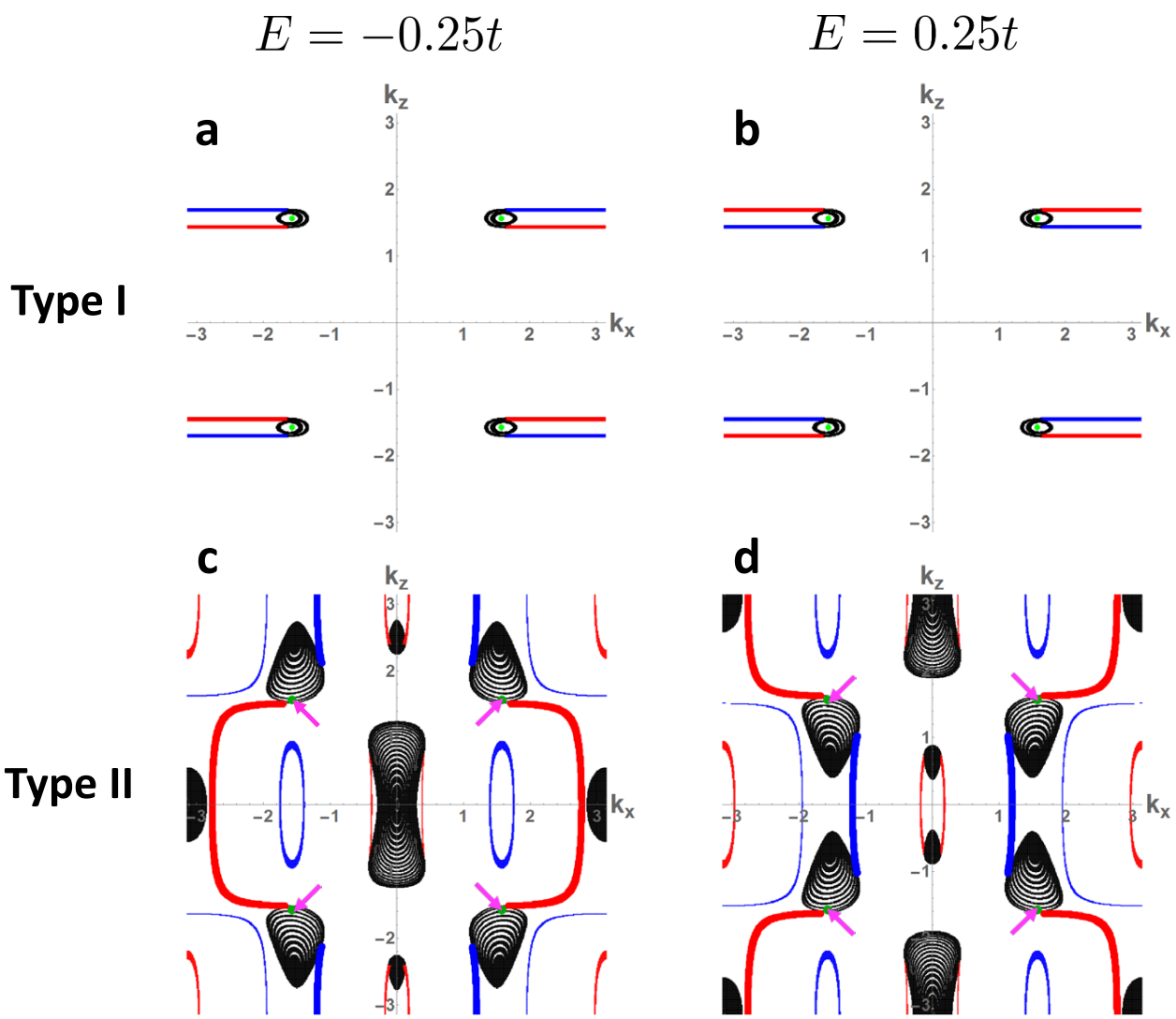

FIG. 7. **Fermi surface and Fermi arc configuration for type-I and type-II inversion-breaking Weyl semimetal. a,b** The Fermi surface and Fermi arc configuration for the Hamiltonian given in Eqn. (11) in the type-I limit ($\gamma = 0$) calculated in a slab geometry with $L = 50$ layers and with bulk parameters the same as in Fig. 6a,d,g. We show this calculation at constant energies: $E = -0.25t$ (**a**) and $E = 0.25t$ (**b**). Here we see that Weyl nodes located at $(k_x, k_z) = (\pm\pi/2, \pm\pi/2)$ are connected by surface states (red and blue lines) to one of opposite chirality across the Brillouin zone in the k_x-direction. **c,d** The Fermi surface and Fermi arc configuration for the Hamiltonian given in Eqn. (11) in the type II limit ($\gamma = 2.4t$) calculated in a slab geometry with $L = 50$ layers and with bulk parameters the same as in Fig. 6c,f,i. We show these for the same constant energies as above: (**c**) and $E = 0.25t$ (**d**). The locations of the Weyl nodes are marked with pink arrows. We term the exponentially localized surface states that form closed loops "track states". Fermi arcs are shown as bold lines and connect Weyl nodes in the k_z-direction.

a set of Fermi pockets such that the only gapped 2D subspace of the Brillouin zone surrounding it contains a net chirality $\chi_{tot} = 0$, then the net chirality of Fermi arcs on a surface is also zero, even though Weyl nodes are present at the Fermi energy. This is illustrated in Fig. 3e where two Weyl nodes of opposite chirality connect a single pair of hole and electron pockets and Fermi arcs are absent even at the nodal energy. However, when the net chirality of nodes connecting the set of pockets is nonzero, then a set of Fermi arcs with net chirality χ_{tot} must satisfy is that they must terminate somewhere on the set of Fermi pockets. This has the striking consequence that even when the Fermi level lies at the node energy and topologically protected Fermi arcs are present, the termination of the surface arcs on the bulk pockets can occur at any point on the surrounding Fermi pockets. We see this illustrated

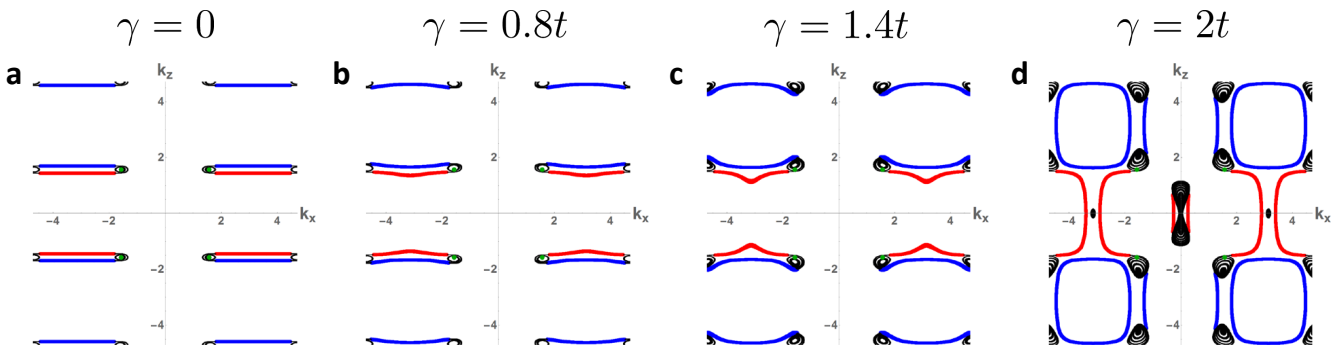

FIG. 8. **Evolution of Fermi surface and Fermi arc configuration for inversion-breaking Weyl semimetal as a function of γ. a-d** The evolution of the Fermi surface and Fermi arc configuration in a slab geometry for Eqn. (11). Bulk states are down in black, surface states are shown in red and blue. We have chosen the parameters $k_0 = \pi/2$, $t_x = t/2$, $m = 2t$. The calculations are done at constant energy $E = -0.25t$ for $\gamma = 0$ (**a**), $\gamma = 0.8t$ (**b**), $\gamma = 1.4t$ (**c**), and $\gamma = 2$. (**d**) shown in an extended Brillouin zone where both k_x and k_z range from -1.5π to 1.5π. We see that at the critical point between a type-I and type-II (**d**), the Fermi arcs that previously connected Fermi pockets in the k_x-direction now connect Fermi pockets in the k_z-direction and track states have formed on the bottom surface (blue) around the $(k_x, k_z) = (\pi, \pi)$ point.

for type-II Weyl nodes connecting isolated pairs of electron and hole pockets in Fig. 5b,e, where the Fermi level is at the Weyl energy but Fermi arcs terminate on a bulk pocket a substantial fraction of a reciprocal lattice vector from the Weyl nodes.

B. Surface "Track States" in Type-II Weyl Semimetals

Topological Fermi arcs are not the only novel surface states possible in a type-II Weyl semimetal. We have shown that due to the finite density of states available at type-II Weyl nodes, new surface states can be appear which we term "track states." These track states are degenerate with the Fermi arcs but do not share the topological properties of the arcs; instead track states form closed contours on a given surface which are contractible to points in the Brillouin zone. Although topologically trivial, track states appear to play an important role in determining the locations Fermi arcs may appear in the surface Brillouin zone.

Track states are generated when the connectivity of Weyl nodes changes as we tune the parameters of a system with multiple pairs of Weyl nodes. In Fig. 8, we see that by tuning the parameter γ in the Hamiltonian in Eqn. (11) through the type-I to type-II transition, the Fermi arcs shift locations. When the nodes are type-I, Fermi arcs pair up nodes of opposite chirality in the k_x-direction; when the nodes are type-II, Fermi arcs pair up nodes in the k_z-direction. Because the Berry curvature is invariant with respect to γ, the Chern number of a bulk-gapped 2D subspace of the Brillouin zone surrounding an isolated node does not change. Although the Fermi arcs can shift locations in the Brillouin zone, the net chirality of modes on a given surface is conserved. When $\gamma = 2t$, track states appear at the (k_x, k_z) points where Fermi arcs were located in the type-I limit.

In a type-II Weyl semimetal, track states can also appear as the Fermi energy shifts. It is shown in Fig. 7c,d that as the Fermi energy changes from below the Weyl energy in Fig. 7c to above the Weyl energy in Fig. 7d, the locations of the arcs shift. For $E < 0$, the arcs on the bottom surface (shown as thick blue contours) connect across the $k_z = \pi$ line while track states are seen as closed blue contours encircling the points $(k_x, k_z) = (\pm\pi/2, 0)$ points. For $E > 0$, this pair of track states have become a single track state encircling the $(k_x, k_z) = (\pm\pi, 0)$ point and a pair of arcs connecting electron pockets across the $k_z = 0$ line. A precisely analogous reconfiguration of states on the top surface also occurs as shown by the reorientation of the red contours.

We note that these track states can appear very similar to Fermi arcs when track states and arcs lie close together. Caution must therefore be taken when analyzing the surface Fermi state configurations of type-II Weyl semimetals in DFT calculations or in ARPES data. There is experimental evidence for the existence of track states in $MoTe_2$[24], WTe_2[49–51], and a recent ARPES study of Ta_3As_2[52] has revealed closed contours of surface states which are strong track state candidates. The Ta_3As_2 system is particularly promising as it has been predicted that pressure can tune a type-I to type-II transition where track states are likely to appear.

VI. COMPARISON WITH EXPERIMENTS

In this section, we describe the current state of experimental realizations of topological Weyl semimetals. Our results are summarized by Table I. Although various ab-inito studies have proven useful in the study of the materials in Table I, as well as the prediction of a variety

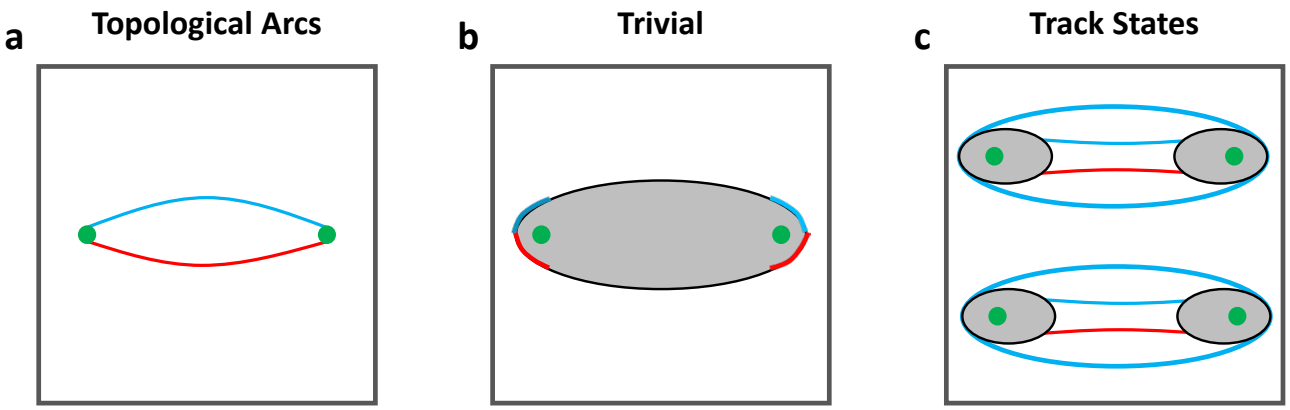

FIG. 9. **Sketch of the three types of surface states in a topological Weyl semimetal.** **a** Two type-I Weyl nodes of opposite chirality connected by a Fermi arc on the top (red) and bottom (blue) surfaces. In an arbitrary type-II TWS at an energy away from the Weyl energy, these arcs would connect Fermi pockets instead of nodes. **b** A single Fermi pocket enclosing two nodes of opposite chirality. Since no Gaussian surface can be constructed in a region that is both gapped and encloses only one node, the only possible surface states are trivial ones, shown in red and blue at the boundary of the pocket that hybridize with bulk states due to lack of topological protection. **c** Pairs of Weyl nodes, two of each chirality with each node surrounded by a Fermi pocket. The pockets are connected by Fermi arcs (thinner red and blue contours) as well as track states (thicker blue lines) on the bottom surface. Note that states on opposite sides of a given loop of track states will disperse in opposite directions and so a Gaussian surface enclosing a given Fermi pocket will still have one net surface state of each chirality.

of Weyl semimetals yet to be discovered experimentally, it is clear that there is a distinct need for a set of minimal models which describe the general features of topological Weyl semimetals. From the abundance of type II TWS in Table I, it is particularly evident that our models provide a general framework for understanding the topological features of type II TWS which is complimentary to DFT.

In Table I, we note that other than the transition metal monophosphides, all of the Weyl semimetals which have been uncovered by spectroscopic experiments are of type II. Additionally, they all break inversion symmetry with strictly more than the minimum of two pairs of nodes. For this reason, we expect track states may be common in Weyl semimetals. Indeed, we have found that a detailed examination of the spectroscopic results indicate that evidence of track states is found in nearly all of the type II Weyl semimetals so far discovered.

The transition metal dichalcogenides $MoTe_2$ and WTe_2 each feature long surface states which begin on bulk electron pockets and terminate on bulk hole pockets. These bulk pockets each enclose the projections of a net zero chirality of Weyl nodes and, by the arguments in Section V above, cannot have a nonzero net chirality of Fermi arcs terminating on it. This is borne out in both the ab-initio calculations as well as the ARPES results[24,49–51]. The long surface state in WTe_2 has been shown[51] to have both topological and trivial character, depending on the material parameters used in the ab-initio calculations and therefore the configurations of the Weyl nodes. This is manifestly a characteristic of a track state.

The transition metal pnictide Ta_3S_2 features[54] 4 pairs of Weyl nodes which are formed from the merging of two hole pockets with an electron pocket. As we have shown in Sec. V above, in such a configuration, there cannot exist a closed and gapped region of the Brillouin zone which encloses a net chirality of Weyl nodes. In this way, all surface states shown in Fig. 4 of Ref.[54] are in fact trivial in a topological sense. Additionally, Ta_3S_2 has set of surface states that lie close in momentum to the bulk hole pockets. The bulk band structure of Ta_3S_2 is predicted to be highly tunable and is has been predicted[54] that strain can tune transitions between type I and type II Weyl semimetals as well as between these semimetal phases and a strong topological insulating phase. It is possible that the track state nature of these surface states will be revealed by such an experiment.

VII. CONCLUSIONS

The models we present here comprehensively describe the four classes of Weyl semimetals which can be delineated by the type of the nodes and whether they break inversion or time-reversal symmetry. Examples from each class have been predicted by theory and have been experimentally observed in quantum materials. Particular realizations obey point group symmetries different in general than those presented here. It is straightforward to extend the models we present here to study a Weyl semimetal with a chosen point group symmetry.

This summary of minimal models for type-I and type-II Weyl semimetals for both time-reversal-breaking and inversion-breaking cases may contribute to future inves-

Material	Type	Broken symmetry	Pairs of Weyl nodes	Surface states
TaAs[13–15], TaP[16], NbAs[REF], NbP[53]	I	Inversion	12	
$MoTe_2$[24]	II	Inversion	4	possible track states
WTe_2[49–51]	II	Inversion	4	possible track states
LaAlGe[25]	II	Inversion	20	
Ta_3S_2[54]	II	Inversion	4	long Fermi arcs, possible track states

TABLE I. Experimental realizations of Weyl semimetals.

tigations of their properties in applied electric and magnetic fields. In particular, we expect our models to shed light on the nature of quantum oscillations in type-II Weyl semimetals. Preliminary calculations[19] show the absence of a chiral zero-energy Landau level when the direction of the applied magnetic field lies outside of the tilt cone of the type-II Weyl node. However, these calculations rely on a linearized model for type-II Weyl nodes and a proper treatment should include the full Fermi pockets surrounding the Weyl nodes. The models presented here provide an ideal framework for such a calculation which we leave for future study. These models also provide a foundation for additional effects of repulsive and attractive interactions. Experimental discoveries of magnetism and superconductivity in Weyl semimetals could provide impetus for such theoretical studies.

ACKNOWLEDGMENTS

The authors would like to thank B. Huang, M. Kargarian and Y.-M. Lu for useful discussions. We would also like to thank A. Kaminski for our collaboration with him on the ARPES study of type II TWS in $MoTe_2$, which inspired much of this work. T. M. M. acknowledges funding from NSF-DMR-1309461 and N. T. was supported by the Center for Emergent Materials, an NSF MRSEC, under grant DMR-1420451. N.T. acknowledges partial support by a grant from the Simons Foundation (# 343227).

* mccormick.288@osu.edu
† itamark@mit.edu
‡ trivedi.15@osu.edu

[1] M. Z. Hasan and C. L. Kane, Rev. Mod. Phys. **82**, 3045 (2010).
[2] X.-L. Qi and S.-C. Zhang, Rev. Mod. Phys. **83**, 1057 (2011).
[3] A. H. Castro Neto, F. Guinea, N. M. R. Peres, K. S. Novoselov, and A. K. Geim, Rev. Mod. Phys. **81**, 109 (2009).
[4] T. D. C. Bevan, A. J. Manninen, J. B. Cook, J. R. Hook, H. E. Hall, T. Vachaspati, and G. E. Volovik, Nature **386**, 689 (1997).
[5] D. Hsieh, D. Qian, L. Wray, Y. Xia, Y. S. Hor, R. J. Cava, and M. Z. Hasan, Nature **452**, 970 (2008).
[6] A. A. Burkov and L. Balents, Phys. Rev. Lett. **107**, 127205 (2011).
[7] X. Wan, A. M. Turner, A. Vishwanath, and S. Y. Savrasov, Phys. Rev. B **83**, 205101 (2011).
[8] G. Xu, H. Weng, Z. Wang, X. Dai, and Z. Fang, Phys. Rev. Lett. **107**, 186806 (2011).
[9] G. Volovik and M. Zubkov, Nuclear Physics B **881**, 514 (2014).
[10] H. Weng, X. Dai, and Z. Fang, Journal of Physics: Condensed Matter **28**, 303001 (2016).
[11] H. Nielsen and M. Ninomiya, Physics Letters B **105**, 219 (1981).
[12] S.-Y. Xu, I. Belopolski, N. Alidoust, M. Neupane, G. Bian, C. Zhang, R. Sankar, G. Chang, Z. Yuan, C.-C. Lee, S.-M. Huang, H. Zheng, J. Ma, D. S. Sanchez, B. Wang, A. Bansil, F. Chou, P. P. Shibayev, H. Lin, S. Jia, and M. Z. Hasan, Science **349**, 613 (2015).
[13] B. Q. Lv, H. M. Weng, B. B. Fu, X. P. Wang, H. Miao, J. Ma, P. Richard, X. C. Huang, L. X. Zhao, G. F. Chen, Z. Fang, X. Dai, T. Qian, and H. Ding, Phys. Rev. X **5**, 031013 (2015).
[14] B. Q. Lv, N. Xu, H. M. Weng, J. Z. Ma, P. Richard, X. C. Huang, L. X. Zhao, G. F. Chen, C. E. Matt, F. Bisti, V. N. Strocov, J. Mesot, Z. Fang, X. Dai, T. Qian, M. Shi, and H. Ding, Nat Phys **11**, 724 (2015).
[15] S.-Y. Xu, N. Alidoust, I. Belopolski, Z. Yuan, G. Bian, T.-R. Chang, H. Zheng, V. N. Strocov, D. S. Sanchez, G. Chang, C. Zhang, D. Mou, Y. Wu, L. Huang, C.-C. Lee, S.-M. Huang, B. Wang, A. Bansil, H.-T. Jeng, T. Neupert, A. Kaminski, H. Lin, S. Jia, and M. Zahid Hasan, Nat Phys **11**, 748 (2015).
[16] S.-Y. Xu, I. Belopolski, D. S. Sanchez, C. Zhang, G. Chang, C. Guo, G. Bian, Z. Yuan, H. Lu, T.-R. Chang, P. P. Shibayev, M. L. Prokopovych, N. Alidoust, H. Zheng, C.-C. Lee, S.-M. Huang, R. Sankar, F. Chou, C.-H. Hsu, H.-T. Jeng, A. Bansil, T. Neupert, V. N. Strocov, H. Lin, S. Jia, and M. Z. Hasan, Science Advances **1** (2015), 10.1126/sciadv.1501092.
[17] Z. K. Liu, L. X. Yang, Y. Sun, T. Zhang, H. Peng, H. F. Yang, C. Chen, Y. Zhang, Y. F. Guo, D. Prabhakaran, M. Schmidt, Z. Hussain, S.-K. Mo, C. Felser, B. Yan, and Y. L. Chen, Nat Mater **15**, 27 (2016).

[18] I. Belopolski, S.-Y. Xu, D. S. Sanchez, G. Chang, C. Guo, M. Neupane, H. Zheng, C.-C. Lee, S.-M. Huang, G. Bian, N. Alidoust, T.-R. Chang, B. Wang, X. Zhang, A. Bansil, H.-T. Jeng, H. Lin, S. Jia, and M. Z. Hasan, Phys. Rev. Lett. **116**, 066802 (2016).

[19] A. A. Soluyanov, D. Gresch, Z. Wang, Q. Wu, M. Troyer, X. Dai, and B. A. Bernevig, Nature **527**, 495 (2015).

[20] Z. Wang, D. Gresch, A. A. Soluyanov, W. Xie, S. Kushwaha, X. Dai, M. Troyer, R. J. Cava, and B. A. Bernevig, Phys. Rev. Lett. **117**, 056805 (2016).

[21] G. Autès, D. Gresch, M. Troyer, A. A. Soluyanov, and O. V. Yazyev, Phys. Rev. Lett. **117**, 066402 (2016).

[22] T.-R. Chang, S.-Y. Xu, G. Chang, C.-C. Lee, S.-M. Huang, B. Wang, G. Bian, H. Zheng, D. S. Sanchez, I. Belopolski, N. Alidoust, M. Neupane, A. Bansil, H.-T. Jeng, H. Lin, and M. Zahid Hasan, Nat Commun **7** (2016).

[23] I. Belopolski, S.-Y. Xu, Y. Ishida, X. Pan, P. Yu, D. S. Sanchez, H. Zheng, M. Neupane, N. Alidoust, G. Chang, T.-R. Chang, Y. Wu, G. Bian, S.-M. Huang, C.-C. Lee, D. Mou, L. Huang, Y. Song, B. Wang, G. Wang, Y.-W. Yeh, N. Yao, J. E. Rault, P. Le Fèvre, F. m. c. Bertran, H.-T. Jeng, T. Kondo, A. Kaminski, H. Lin, Z. Liu, F. Song, S. Shin, and M. Z. Hasan, Phys. Rev. B **94**, 085127 (2016).

[24] L. Huang, T. M. McCormick, M. Ochi, Z. Zhao, M.-T. Suzuki, R. Arita, Y. Wu, D. Mou, H. Cao, J. Yan, N. Trivedi, and A. Kaminski, Nat Mater **15**, 1155 (2016).

[25] S.-Y. Xu, N. Alidoust, G. Chang, H. Lu, B. Singh, I. Belopolski, D. Sanchez, X. Zhang, G. Bian, H. Zheng, M.-A. Husanu, Y. Bian, S.-M. Huang, C.-H. Hsu, T.-R. Chang, H.-T. Jeng, A. Bansil, V. N. Strocov, H. Lin, S. Jia, and M. Z. Hasan, "Discovery of lorentz-violating weyl fermion semimetal state in laalge materials," (2016), arXiv:1603.07318.

[26] P. Delplace, J. Li, and D. Carpentier, EPL (Europhysics Letters) **97**, 67004 (2012).

[27] T. Ojanen, Phys. Rev. B **87**, 245112 (2013).

[28] M.-C. Chang and M.-F. Yang, Phys. Rev. B **91**, 115203 (2015).

[29] P. Hosur, S. A. Parameswaran, and A. Vishwanath, Phys. Rev. Lett. **108**, 046602 (2012).

[30] D. T. Son and B. Z. Spivak, Phys. Rev. B **88**, 104412 (2013).

[31] Y. Chen, S. Wu, and A. A. Burkov, Phys. Rev. B **88**, 125105 (2013).

[32] H.-J. Kim, K.-S. Kim, J.-F. Wang, M. Sasaki, N. Satoh, A. Ohnishi, M. Kitaura, M. Yang, and L. Li, Phys. Rev. Lett. **111**, 246603 (2013).

[33] M. M. Vazifeh and M. Franz, Phys. Rev. Lett. **111**, 027201 (2013).

[34] M. Kargarian, M. Randeria, and N. Trivedi, Scientific Reports **5**, 12683 (2015).

[35] C. J. Tabert and J. P. Carbotte, Phys. Rev. B **93**, 085442 (2016).

[36] A. C. Potter, I. Kimchi, and A. Vishwanath, Nat Commun **5**, 5161 (2014).

[37] B. Z. Spivak and A. V. Andreev, Phys. Rev. B **93**, 085107 (2016).

[38] R. Lundgren, P. Laurell, and G. A. Fiete, Phys. Rev. B **90**, 165115 (2014).

[39] G. Sharma, P. Goswami, and S. Tewari, Phys. Rev. B **93**, 035116 (2016).

[40] J. Klier, I. V. Gornyi, and A. D. Mirlin, Phys. Rev. B **92**, 205113 (2015).

[41] P. Goswami, J. H. Pixley, and S. Das Sarma, Phys. Rev. B **92**, 075205 (2015).

[42] M. Koshino and I. F. Hizbullah, Phys. Rev. B **93**, 045201 (2016).

[43] A. Altland and D. Bagrets, Phys. Rev. Lett. **114**, 257201 (2015).

[44] A. Altland and D. Bagrets, Phys. Rev. B **93**, 075113 (2016).

[45] D. A. Pesin, E. G. Mishchenko, and A. Levchenko, Phys. Rev. B **92**, 174202 (2015).

[46] M. O. Goerbig, J.-N. Fuchs, G. Montambaux, and F. Piéchon, Phys. Rev. B **78**, 045415 (2008).

[47] K.-Y. Yang, Y.-M. Lu, and Y. Ran, Phys. Rev. B **84**, 075129 (2011).

[48] D. J. Thouless, M. Kohmoto, M. P. Nightingale, and M. den Nijs, Phys. Rev. Lett. **49**, 405 (1982).

[49] C. Wang, Y. Zhang, J. Huang, S. Nie, G. Liu, A. Liang, Y. Zhang, B. Shen, J. Liu, C. Hu, Y. Ding, D. Liu, Y. Hu, S. He, L. Zhao, L. Yu, J. Hu, J. Wei, Z. Mao, Y. Shi, X. Jia, F. Zhang, S. Zhang, F. Yang, Z. Wang, Q. Peng, H. Weng, X. Dai, Z. Fang, Z. Xu, C. Chen, and X. J. Zhou, Phys. Rev. B **94**, 241119 (2016).

[50] Y. Wu, D. Mou, N. H. Jo, K. Sun, L. Huang, S. L. Bud'Ko, P. C. Canfield, and A. Kaminski, Phys. Rev. B **94**, 121113 (2016).

[51] F. Y. Bruno, A. Tamai, Q. S. Wu, I. Cucchi, C. Barreteau, A. De La Torre, S. McKeown Walker, S. Ricco, Z. Wang, T. K. Kim, M. Hoesch, M. Shi, N. C. Plumb, E. Giannini, A. A. Soluyanov, and F. Baumberger, Phys. Rev. B **94**, 121112 (2016).

[52] G. Chang, S.-Y. Xu, D. S. Sanchez, S.-M. Huang, C.-C. Lee, T.-R. Chang, G. Bian, H. Zheng, I. Belopolski, N. Alidoust, H.-T. Jeng, A. Bansil, H. Lin, and M. Z. Hasan, Science Advances **2** (2016), 10.1126/sciadv.1600295.

[53] S. Souma, Z. Wang, H. Kotaka, T. Sato, K. Nakayama, Y. Tanaka, H. Kimizuka, T. Takahashi, K. Yamauchi, T. Oguchi, K. Segawa, and Y. Ando, Phys. Rev. B **93**, 161112 (2016).

[54] G. Chang, S.-Y. Xu, D. S. Sanchez, S.-M. Huang, C.-C. Lee, T.-R. Chang, G. Bian, H. Zheng, I. Belopolski, N. Alidoust, H.-T. Jeng, A. Bansil, H. Lin, and M. Z. Hasan, Science Advances **2** (2016), 10.1126/sciadv.1600295.